TIME VARIABILITY OF CIRCINUS X-1

By

© CHRISTOPHER FRANK HAYES, B.Sc.

A Thesis

Submitted to the School of Graduate Studies

in Partial Fulfilment of the Requirements

for the Degree

Master of Science

McMaster University

August 1980

TIME VARIABILITY OF CIRCINUS X-1

MASTER OF SCIENCE (1980)
(Physics)

McMASTER UNIVERSITY
Hamilton, Ontario

TITLE: Time Variability of Circinus X-1

AUTHOR: Christopher Frank Hayes, B.Sc. (McMaster University)

SUPERVISOR: Professor Peter G. Sutherland

NUMBER OF PAGES: v, 54

ABSTRACT

The current interest in the X-ray source Circinus X-1 stems from its similarity to Cygnus X-1, the prime black hole candidate. In this thesis Circinus X-1 will be examined in terms of time variability from data obtained by the first High Energy Astronomy Observatory (HEAO-1) during August 1977. The study involves the determination of time averaged characteristics in the form of statistical moments, hardness ratios, and correlation functions. Also included is a brief history of X-ray astronomy, the energetics of X-ray emission from compact stellar objects, followed by a description of the HEAO-1 satellite and a review of previous work on Circinus X-1 and Cygnus X-1.

ACKNOWLEDGEMENTS

I would like to extend many thanks to my supervisor, Dr. Peter G. Sutherland, for his helpful guidance and enthusiastic encouragement.

My thanks to Kent Wood and his colleagues at the Naval Research Labs in Washington for assistance with the initial data tapes.

Victory in the battle against the computer was achieved with the aid of comrades-in-arms Bob Jaskula and desk mate Eugene Cohler.

I have enjoyed many interesting conversations in, around, and out of physics with members of the Theory Group, primarily Graham Glen and other companions of the Tuesday Night Pizza Club; Anup Dutta, Boza Mitrović, and Zoltan Racz.

I would also like to express my appreciation to the indispensable Mrs. Helen Kennelly for her incredibly quick and accurate typing of this thesis.

TABLE OF CONTENTS

" ... "Guilt by association" ... there's a very real danger that we would actually convict the innocent and fail even to indict the guilty."

- F. Lamb

I. INTRODUCTION

In most subjects there are particular elements that can be termed "exotic", having an attraction based on the unusual. In X-ray astronomy the exotic includes the family of "collapsed" stars: white dwarfs, neutron stars, and black holes. The theoretical and observational characteristics of these extremely dense objects are the subject of much current research in astrophysics.

Collapsed stars are expected as possible endpoints of stellar evolution. These objects are formed upon exhaustion of nuclear fuels, when thermal pressure can no longer be maintained to withstand gravity. The central stellar cores collapse to high densities where the degeneracy pressure of fermions (electrons for white dwarfs, neutrons for neutron stars) can balance gravity. If the core mass is too large, no thermal or degeneracy pressure is large enough, gravity wins and a black hole is formed. Their formation produces a deep gravitational well so that if the large kinetic energy that is gained by infalling material is thermalized, then copious X-ray emission results. This process is believed to be responsible for the X-ray generation of many galactic sources including Circinus X-1.

The study of X-ray emitting objects encounters difficulties that are alien to optical astronomy. Atmospheric absorption of X-rays forces the use of balloons, rockets, or satellites in any research attempt. Source location with an accuracy comparable to that of optical astronomy has only recently been attained with the X-ray telescope of the Einstein Observatory. Collection and interpretation of spectral data, while reasonably straightforward optically, is severely limited by the low resolution of gas proportional counters. In addition, the high temperature X-ray emission regions involve complex and poorly understood processes. It follows that the analytical results of such spectral data are vague and possibly misleading. Therefore, the prime area of X-ray astronomical research dealing with point-like sources is time variability. It allows an interesting and informative look at the underlying physical processes of stellar X-ray emission with the significant advantage that it is distance independent.

Circinus X-1 is a strong, "noisy", discrete, galactic X-ray source that exhibits a variability over a large range of time scales. It has been optically identified with a red star that is sufficiently faint to make spectral analysis and the determination of binary parameters difficult. Time variability studies are ideally suited to these conditions. With millisecond fluctuations, flares, and an eclipse-like 16.6 d period, the source is particularly interesting since

its X-ray emission is similar to that of Cygnus X-1, the prime black hole candidate. The analysis of Circinus X-1 may lead to a better understanding of the processes behind X-ray emission and in turn aid in the classification of collapsed stars and X-ray sources in general.

A. History of X-ray Astronomy

The problem of overcoming the atmospheric barriers to X-rays was first successfully approached in 1948 by an American-launched V2 rocket experiment (Burnight, 1949) that established soft X-ray emission from the solar corona. The results also indicated that such a low signal would be undetectable at stellar distances. It was not until 1962 that the first extrasolar signal was detected from the constellation of Scorpius (Giacconi et al. 1962). The source, Sco X-1, is the strongest constant X-ray emitter in the sky with an X-ray luminosity $\sim 10^{37}$ erg s^{-1}. It was also the first source to be optically identified (Sandage et al. 1966). During this time the Crab Nebula, known to be active in the optical and radio frequencies, was discovered to be an X-ray emitter (Bowyer et al. 1964), containing at its center a supernova remnant. This was followed by the discovery of the first extragalactic X-ray source, the giant elliptical galaxy M87 (Byram et al. 1966).

Further work during the decade incorporated the use of rockets and balloons. Their restrictions, such as short data acquisition time and limited X-ray detection were largely

superceded with the December 1970 launching of the Small Astronomy Satellite (SAS-1, also known as Uhuru), the first satellite to be designed specifically for X-ray astronomical research. The payload consisted mainly of sky sensors and two proportional counters with a total area of 1680 cm^2 and a $0°.52 \times 5°.2$ and $5°.2 \times 5°.2$ collimated field of view (Giacconi et al. 1971). The resulting 3U catalogue contained 162 sources. Later the revised catalogue (4U) contained 339 sources.

Other satellites followed such as the British Ariel V with its All Sky Monitor (ASM) capable of scanning the celestial sphere at all times, the Astronomical Netherland Satellite (ANS), SAS-3, and in 1977 the first High Energy Astronomy Observatory (HEAO-1).

In the past decade, therefore, numerous satellites have been used to collect a vast amount of information on the X-ray sky. The data have enabled a general classification scheme of X-ray sources to be formed which will be briefly outlined.

B. X-ray Sources

Beyond the Sun, X-ray sources fall into the two broad categories of galactic and extragalactic.

Extragalactic Sources

Extragalactic sources vary from being discrete, such as SMC X-1 in the Small Magellanic Cloud, to extended objects in clusters of galaxies with dimensions from a few hundred to a few thousand parsecs (Kellog 1973). Their energy output is

typically several orders of magnitude greater than those of galactic origin lying in the range $10^{41} - 10^{46}$ erg s^{-1} and perhaps are the source of the isotropic background above a few keV (Gursky et al. 1963). Unfortunately detectors with reasonable spatial resolving power and sensitivity are only now becoming available so that detailed information on the structure of extragalactic sources is, at present, scarce. Although a good understanding of the physics of X-ray sources will probably come from galactic work, the extragalactic region will play a significant role in furthering the study of galaxy formation and evolution, intergalactic matter and other questions of importance to astrophysics and cosmology.

Galactic Sources

With the exception of Sco X-1 and Her X-1 with flux densities of $\sim 10^{-7}$ erg $cm^{-2}s^{-1}$ and $\sim 10^{-9}$ erg cm^{-2} s^{-1} respectively, the strongest galactic sources are found close to the plane of the galaxy and in the galactic bulge. They have an X-ray luminosity in the range $10^{31} - 10^{38}$ erg s^{-1} (2-11 keV) and contribute to an estimated galactic emission of $\sim 5\times10^{39}$ erg s^{-1} in the 2-10 keV range. Most of these galactic sources can be classified by their temporal structure varying from the millisecond level to years.

Pulsating eclipsing binaries have massive and highly luminous optical companions. The X-ray source itself gives a pulsed signal with a period of seconds indicating a compact

object with a magnetic field, possibly a white dwarf or neutron star. The optical source is seen to have a varying flux possibly due to tidal forces and/or X-ray heating by the compact star. The changing flux aids in the identification of the X-ray optical pair.

An example is Centaurus X-3 (Cen X-3), with a pulse period of 4.8 s, and an O-type optical companion (Osmer et al. 1975) that eclipses the source every 2.087 days. Other examples of this type include Vela X-1, 4U1538-52 and Her X-1.

Non-eclipsing binaries have a larger X-ray to optical luminosity ($L_x/L_\odot \sim 1000$) than pulsating eclipsing binaries. Their spectrum is flat with a strong ultraviolet component. Only one of this type has been found to pulsate (4U1627-67 with period $\tau = 7.68$ s). It is believed in this case that the system is a low mass tight binary containing a compact object (likely a neutron star) with a non-degenerate dwarf primary. Since the orbital period is less than 0.2 days the Doppler shift is difficult to measure. The first detected extrasolar source Sco X-1 is also a member of this group.

Transients, as indicated by their name, occur suddenly in regions previously devoid of strong X-ray emission. Transients appear suddenly, their flux rising to a peak in approximately a week and then gradually decreasing over a period of months. Some have been observed to pulse with a hard spectra, while others have soft spectra followed by an increase in the optical output of the companion. Recent observations of Centaurus X-4 (Cani-

zares et al. 1980) indicate transients differ from bursters mainly in the time interval between bursts, generally months to years.

Bursters are characterized by a sudden (∿ few seconds) increase in X-ray flux followed by a flux decrease over a few minutes. Time intervals between bursts, from hours to days, define the slow bursters of which ∿ 30 are known (e.g. MXB 1728-34). Only one rapid burster is known, MXB 1730-335, discovered in 1976 (Lewin et al. 1976). It produces small and large bursts on the order of minutes with time intervals between 10 s and 500 s (Lewin et al. 1976), proportional to the energy released in the large bursts.

Supernova remnants (SNR) are distinctly different from the classes previously mentioned. Under certain conditions it is possible for a star to end its life by violently discharging a large portion of its envelope into the interstellar medium. The X-rays radiate from a hot plasma just behind the shock front.

There is one special exception or extension to this class; the Crab Nebula and its associated pulsar. The Crab Nebula is the site of an ∿ 1000 year old supernova explosion. The hot X-ray and optical emitting gas of the region was the first X-ray source to be identified with an optical object (Bowyer et al. 1964). Concurrent with the visible center of the nebula is the source of a strong pulsing X-ray source, the Crab pulsar. The location and the observed pulsation period of 33 ms strongly argues for a highly magnetized rotating

neutron star, the released energy due to synchrotron emission by high energy electrons accelerated in a magnetic field.

Essentially in a category by itself is Cygnus X-1, the prime black hole candidate. Because its X-ray output resembles that of Cir X-1, especially in short time variability, a more detailed summary of its characteristics follows the review of Cir X-1.

C. Energetics

One of the first questions to be considered is: why is it necessary to invoke compact objects as the probable source of most galactic X-rays?

The hottest stars known have an effective blackbody temperature in the tens of thousands of degrees Kelvin. This corresponds to a small X-ray emission in comparison to the visible output. Therefore any normal star that can be detected as an X-ray source should be easily identified optically. This is not the case for the strong X-ray emitters. The standard model suggests that the energy required to produce X-rays is available in the gravitational potential well of a compact object.

The energy gained by a particle of mass m at infinity falling onto a compact object of mass M_x and radius R_x is

$$E = \frac{GM_x m}{R_x} . \qquad (1.1)$$

For an object of mass $\sim M_\odot$ with a radius of a white dwarf ($R_x \sim 10^9$ cm), the energy gained by a hydrogen atom is ~ 100 keV. Equivalently for a neutron star of radius 10^6 cm, the energy is ~ 100 MeV. For a black hole, if the energy emission comes from material that has fallen into $3R_s$, where R_s is the Schwarzschild radius given by

$$R_s = \frac{2GM_x}{c^2} , \tag{1.2}$$

the available energy is ~ 150 MeV per hydrogen atom, for a 1 $M_\odot$ black hole. To compare, a 1 $M_\odot$ main sequence star gives ~ 2 keV per H atom.

The maximum steady X-ray luminosity is not expected to exceed the Eddington limit, where radiation pressure (determined by scattering off electrons) is just balanced by gravity:

$$L_{x,max} = \frac{4\pi GM_x m_p c}{\sigma_T} \sim 10^{38} \frac{M_x}{M_\odot} \text{ erg s}^{-1} ; \tag{1.3}$$

here m_p is the proton mass and σ_T is the Thomson cross-section. Many of the most powerful galactic X-ray sources have luminosities of this order. The required mass accretion rate, $\dot{M}$, is determined by

$$L_x \sim \frac{GM_x\dot{M}}{R_x} \tag{1.4}$$

and thus falls in the range $10^{-8} - 10^{-10}$ $M_\odot$ yr^{-1} for strong sources where the accretion is onto either a neutron star or a

black hole of mass ∿ few solar masses. Because white dwarfs are less compact ($R \sim 10^9$ cm), for a comparable luminosity they require a much larger accretion rate. However, theoretical studies of accretion onto white dwarfs (Fabian et al. 1976) show that even under the most favourable conditions their luminosities cannot exceed 10^{36} erg s^{-1}. Thus they may correspond to weak X-ray sources, but are not viable candidates for a strong source like Cir X-1.

Although the high particle kinetic energies suggested by Eqn. 1.1 are ∿ 100 MeV for neutron stars or black holes, even when such a source operates near the Eddington limit, the energy it radiates will be predominantly in the X-ray band. This is a consequence of the black-body rules. With an emitting area $\sim 4\pi R_x^2$, then

$$L_x \sim L_{x,max} \sim 4\pi R_x^2 \sigma T^4 \qquad (1.5)$$

requires $T \sim 10^7$ K, or photons of energy ∿ few keV.

D. HEAO-1

The ∿ $300 million High Energy Astronomy Observatory project involves a three satellite program designed to survey and map X-ray, gamma ray and cosmic ray sources over the celestial sphere.

The first satellite, HEAO-1 was launched August 12, 1977 into an ∿ 400 km, circular ($\varepsilon = 0.001501$) orbit by an Atlas-Centaur booster. The spacecraft measured 6 m in length by 2.4 m in diameter and weighed 2700 kg. The four experiments aboard

are summarized below.

1) Large X-ray Survey Experiment: Under the guidance of Dr. Herbert Friedman of the Naval Research Labs, the experiment includes the mapping of the celestial sphere of X-rays in the 100 eV to 20 keV region and the acquisition of energy spectra, intensities and time variability of X-ray sources, with emphasis on weak galactic sources. The data that are analysed in this thesis came from this experiment.

2) Cosmic X-ray Experiment: search for diffuse X-rays in the 0.2 to 60 keV range and correlate the investigation with radio and optical emission.

3) Scanning Modulation Collimator Experiment: determine the position, size, and structure of selected cosmic X-ray sources in the 1 to 15 keV range.

4) Hard X-ray and Low Energy Gamma Ray Experiment: determine position, spectrum, time variability, and intensity of X-rays in the 10 keV to 10 MeV range.

The satellite contained a total of 7 X-ray sensor modules, each a gas proportional counter with approximate dimensions of 24 inches by 36 inches filled with a Xe-CH_4 gas mixture. The 4 modules used in the analysis of Cir X-1 gave a 1°×4° field of view (1° in the scan direction) each of an area 1650 cm^2.

The satellite's roll period of ∿ 30 minutes gave ∿ 5 s of on-source data per scan. Two data collecting modes were used.

The scan mode incorporated the use of either a 16 or 40 channel pulse height analyser (PHA), counts being accumulated in 320 ms bins. The point-scan mode bypassed the PHA's with bins reduced to 5 ms for detailed time variability study.

E. Circinus X-1 Review

Cir X-1 (4U1516-56) was first definitely observed on June 14, 1969 (Margon et al. 1971) and possibly earlier by Harries et al.(1971). Its binary nature was first suggested in 1976 (Mayo et al. 1976) from detected H_α emission and was later confirmed by optical, radio (Whelan et al. 1977), and infrared studies (Glass 1978). The optical companion is a faint red star with colour magnitudes $m_J \sim 22.5$ in the blue and $m_R \sim 16$ in the red (Whelan et al. 1977). The low intensity in these bands makes it difficult to obtain binary parameters based on Doppler spectroscopy.

The close proximity (within 16') of the supernova remnant G321.9-0.3 allowed an approximate distance determination between 4 kpc and 9 kpc (Clark et al. 1975). This is consistent with an estimated minimum distance of 4 kpc from optical and radio data (Whelan et al. 1977). Measurements at 21 cm in the December 1976 radio burst produced a firm lower limit at $\sim$ 8 kpc and an estimated upper limit of 16 kpc (Goss and Mebold 1977).

Time Variability

The source is characterized by its variability over time scales from the millisecond level to months. Occasional

flares followed by long periods ($\sim 10^2$ days) below detector threshold are interspersed with sharp transitions (on the order of minutes) to below detectable levels, then gradually rising above threshold in days.

Observations by the OSO-7 satellite between December 10, 1971 and December 4, 1972 (Canizares et al. 1974) showed only one clear incidence above detector threshold. Copernicus satellite data of a 13 h duration showed no detectable emission on June 14, 1973 (Tuohy and Davison 1973). A 130 s rocket experiment on November 9, 1973 (Spada et al. 1974) recorded a low count rate of 0.359 photons cm^{-2} s^{-1} with no significant aperiodic pulsations between 1 ms and 1 s.

Uhuru data between January 1971 and February 1973 (Jones et al. 1974) in the 2-6 keV range exhibited off states lasting from 0.5 d to several days. Although an off state periodicity (12.288±0.015 d) was first suggested here, a predicted off state was not observed in the OSO-7 data, consequently ruling out periods < 15 days. No short term periodicity was identified by Jones et al. (1974) but there was noted a possibility of pulse trains lasting 10's of seconds. Spectral analysis of the Uhuru data showed variations in the low energy cutoff. It was proposed that this could be explained by significant absorption near the source rather than by the interstellar medium.

Observations by the Ariel V Rotation Modulation Collimator (RMC) in February 1976 (Wilson and Carpenter 1976) showed

a burst rising from below detector threshold over 3 days to a peak intensity > 40 counts s^{-1} then declining to below threshold in a few hours. The outburst was confirmed by the Ariel V All Sky Monitor (ASM) (Coe et al. 1976b) which displayed an increase in the soft X-ray flux of at least two orders of magnitude. No corresponding increase in the hard X-ray flux was observed. Further ASM results between October 1975 and April 1976 (Kaluzienski et al. 1976) in the 3-6 keV range showed six periodic eclipse-like transitions to below detector threshold in $\leq$ 0.07 d, later slowly rising to detection level. Their calculated period, 16.585±0.01 d, was verified by SAS-3 data in January 1976 (Buff et al. 1977). The SAS-3 observed transition was immediately (< 2 d) preceded by two flares: a small peak ($\sim$ 25 counts s^{-1}) followed by a larger flare (> 75 counts s^{-1}) reaching 1/2 the intensity of the Crab Nebula. Fluctuations of < 1 s were also noticed. Additional evidence of a 16.6 d period was provided by COS-B satellite data during February and March 1976 (Bignami et al. 1977).

Short time variability on the order of milliseconds was first observed by Toor (1977) on June 6, 1976. A burst of an approximate 40 ms duration rose about five fold over the average count rate. Prior to this, only Cygnus X-1 had exhibited millisecond structure (Rothschild et al. 1974).

Six separate observations near predicted 16.6 d transition dates between October 1976 and October 1977 (Dower, 1978), displayed up to factor of 10 intensity drops followed by low,

but non-zero, count rates. The source became undetectable 1-6 days after transition. One observation in particular dropped by a factor of 5 in luminosity in less than 60 s. In addition, low energy flux was noticed to be strong before transition. On short time scales (2-6 ms), 19 bursts with count rates $\geq$ 50 times the average were reported.

Recent HEAO A-1 data of August 1977 (Sadeh et al. 1979) showed a low count rate followed by an $\sim$ 2 d high state that varied by a factor of 2 in intensity during 15-30 m intervals. Also reported was a single scan with a 2.5 s pulse period detected in a 40 s pulse train. Other unconfirmed periods on the order of seconds had been reported earlier (Margon et al. 1971, Toor 1977).

Some verification of a 16.6 d period exists at radio (Whelan et al. 1977, Goss and Mebold 1977) and infrared frequencies (Glass 1978) in the region of Cir X-1. Whereas the X-ray curve suddenly drops at transition then slowly rises, after a delay of hours to days from the transition both radio and infrared fluxes increase quickly (few hours) then decrease gradually (1-10 days).

Optical variability has also been observed (Whelan et al. 1977) but insufficient data prevents a correlation being made with a 16.6 d period.

Spectral Characteristics

Spectral fits to thermal bremsstrahlung, black-body, and power laws yield varying results, temperatures ranging from

1×10^7 K to 20×10^7 K. Energy power laws give spectral indices in the range of 1-4. Spectral cut-offs in the range 1.5-4 keV correspond to column densities between 1×10^{22} cm^{-2} and 14×10^{22} cm^{-2}. The large difference in cut-off energy may indicate significant absorption at the source (Jones et al. 1974). Several reports (e.g. Coe et al. 1976b, Dower 1978) have noted that pre-transition emission is strong in the lower energy region ($\lesssim$ 10 keV) with no comparable increase in the high energy emission ($\gtrsim$ 10 keV). Recent SAS-3 data (Dower 1978) exhibits a steep spectral index at pre-transition followed by a less steep one several hours into post-transition.

F. Cygnus X-1

Cygnus X-1 was first detected in a series of rocket flights in 1962-63 (Giacconi et al. 1962, Gursky et al. 1963). The source displays aperiodic fluctuations on time scales from seconds down to milliseconds. This source has an optical companion, HDE 226868, which is a 9th magnitude, single line spectroscopic binary with orbital period 5.6 d; it is believed to be a BOIb supergiant at a distance of 2.5 kpc (Murdin and Webster 1971, Rappaport et al. 1971b, Webster and Murdin 1972, Bolton 1972, Walborn 1973). The binary orbit parameters inferred from the periodic Doppler shift of optical lines, together with an expected mass of $\gtrsim$ 10 $M_\odot$ for such a supergiant suggest that the X-ray emitting companion has a mass $M_X \gtrsim 4\ M_\odot$. Other methods of deducing M_X arrive at similar lower limits

(see Bahcall 1978 and references therein). These limits for M_x are the source of much of the interest in Cyg X-1. [There is evidence of a 5.6 d period in the X-ray light curve (Holt et al. 1976a, Holt et al. 1976b) but to date this has not yielded any further constraints on the binary system parameters.] The estimated mass is significantly above the upper limit generally accepted for neutron stars. The high mass, an absence of rotational modulation, and a small spatial extent (indicated by its rapid intensity fluctuations) suggest a black hole as the source of the X-ray emission.

Time Variability

Cyg X-1 undergoes irregular transitions from periods of high flux to extended periods of low flux with intensities in the energy band $\sim$ 1 keV to $\sim$ 20 keV varying by factors between 2 and 4.

After a high flux state between December 1970 and March 1971 there was a transition to the low flux state, accompanied by a factor of 4 decrease in the 2-6 keV range, constant flux between 6 and 10 keV, while the high energy band (10-20 keV) underwent a factor of 2 increase (Tananbaum et al. 1972).

In contrast with the above, the transition back to the high state in May 1975 showed a factor of 5 intensity increase followed by a decay over 22 d (Eyles et al. 1975), where energies over 20 keV displayed a reduction in emission (Coe et al. 1976a).

The high state again returned during the period November 1975 to February 1976. A decrease in the high energy intensity (> 20 keV) was again found (Sommer et al. 1976, Dolan et al. 1977). The source has been in a low flux state since this.

While occasional transitions to the high state are superimposed on a relatively constant low state over the long term, variations on short time scales are markedly irregular. Beyond the absence of pulsing, Cyg X-1 has been seen to flare over a period of seconds (Canizares and Oda 1977) and has exhibited bursts on time scales of 0.640 s (Rothschild et al. 1974), 0.050 s (Rappaport et al. 1971a) and less (Weisskopf et al. 1978). Only Cyg X-1 and Cir X-1 are known to fluctuate at the millisecond level.

II. OBSERVATIONS AND RESULTS

A. Data Base Description

The HEAO-1 data were obtained in two telemetry modes: scan, with a time resolution of 0.320 s, and point-scan, with a time resolution of 0.005 s.

Scan Mode

In this format, all photons detected by the four gas proportional counters (modules 1 to 4) were sorted and accumulated in a 16 channel, non-linear, pulse height analyser (PHA) with a 0.320 s bin size. The PHA spanned the energies 100 eV to 20 keV but the energy range per-channel was not very sharp or stable (primarily because of varying gains in the individual proportional counters). We have not made use of the PHA information beyond separating counts into two energy bands, low (channels 1-11) and high (channels 12-15) corresponding to a split near 6 keV.

A pass of the source lasting $\sim$ 12 s was defined as an "observation". Each observation spanned about one half of a major frame where a major frame is equivalent to 128 minor frames each of which contained the 0.320 s binned data. The peak collimator response (CR) per observation, determined via the aspect solution, served to define the center of the observation about which 64 minor frames were chosen. Approximately 36 minor frames of this were on-source data. The leading

edge of an observation was used to determine background. The trailing edge was not used due to the close proximity of the galactic bulge. With the CR ranging from 0 (off the source) to 1 (directly on source), only 20 minor frames of the on-source data about the peak CR were retained for analysis in order to reduce statistical fluctuations caused by low collimator reponse.

Point-scan Mode

The major and minor frame structure of the 5 ms resolution point-scan data is identical to that of the scan mode with the following exceptions. Detected counts bypassed the 16 channel PHA so that energy sorting into 0.320 s bins was replaced by 64 time sequenced 5 ms bins. The time resolution was therefore enhanced at the expense of spectral resolution.

All observations in either the scan or point-scan mode with a CR < 10% were omitted from the analysis.

The raw form of typical 0.320 s data received from HEAO-1 is illustrated in Figure 1. The total counts per 0.320 s from the 16 channel PHA are plotted against a time axis of total length $\sim$ 20 s. The central triangular shape represents the collimator response due to the scanning motion of the satellite across the source.

Once the CR and background are removed the source fluctuations in both energy bands can be clearly seen (Figure 2) and analytical methods can be applied.

Figure 1 HEAO-1 Raw Data for 1 Observation

This represents a typical scan of 0.320 s data with the collimator response (triangular shape formed by the solid line) included. Errors given are 1σ.

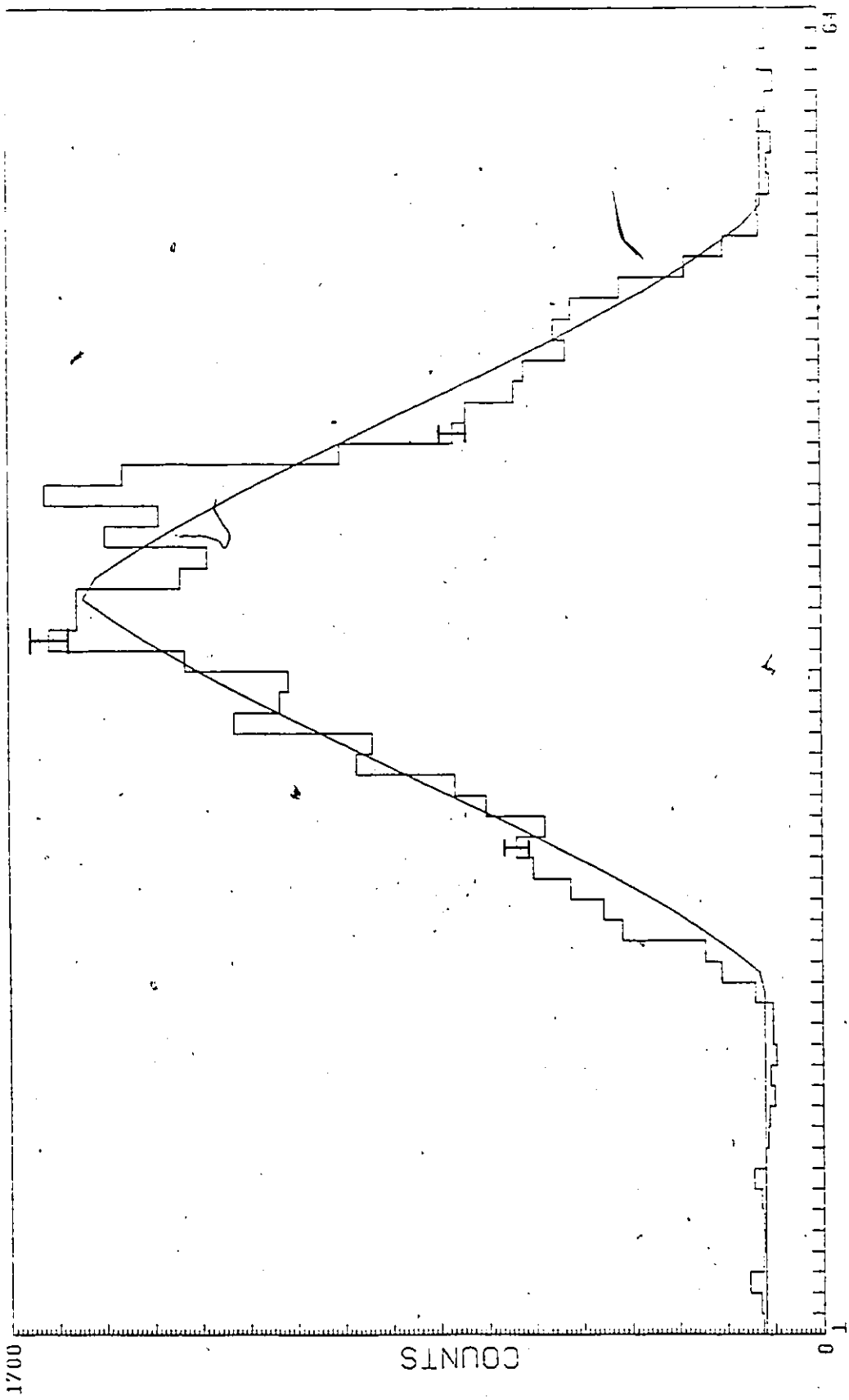
1700
COUNTS
0
1
64
BIN NUMBER

Figure 2. Corrected HEAO-1 Data for 1 Observation

The collimator response and background have been removed from the data illustrated in Figure 1. The upper curve represents those counts in the low energy channels (1-11) of the PHA, the lower one for the high energy channels (12-15). The 20 bins are chosen about the peak collimator response to minimize statistical fluctuations.

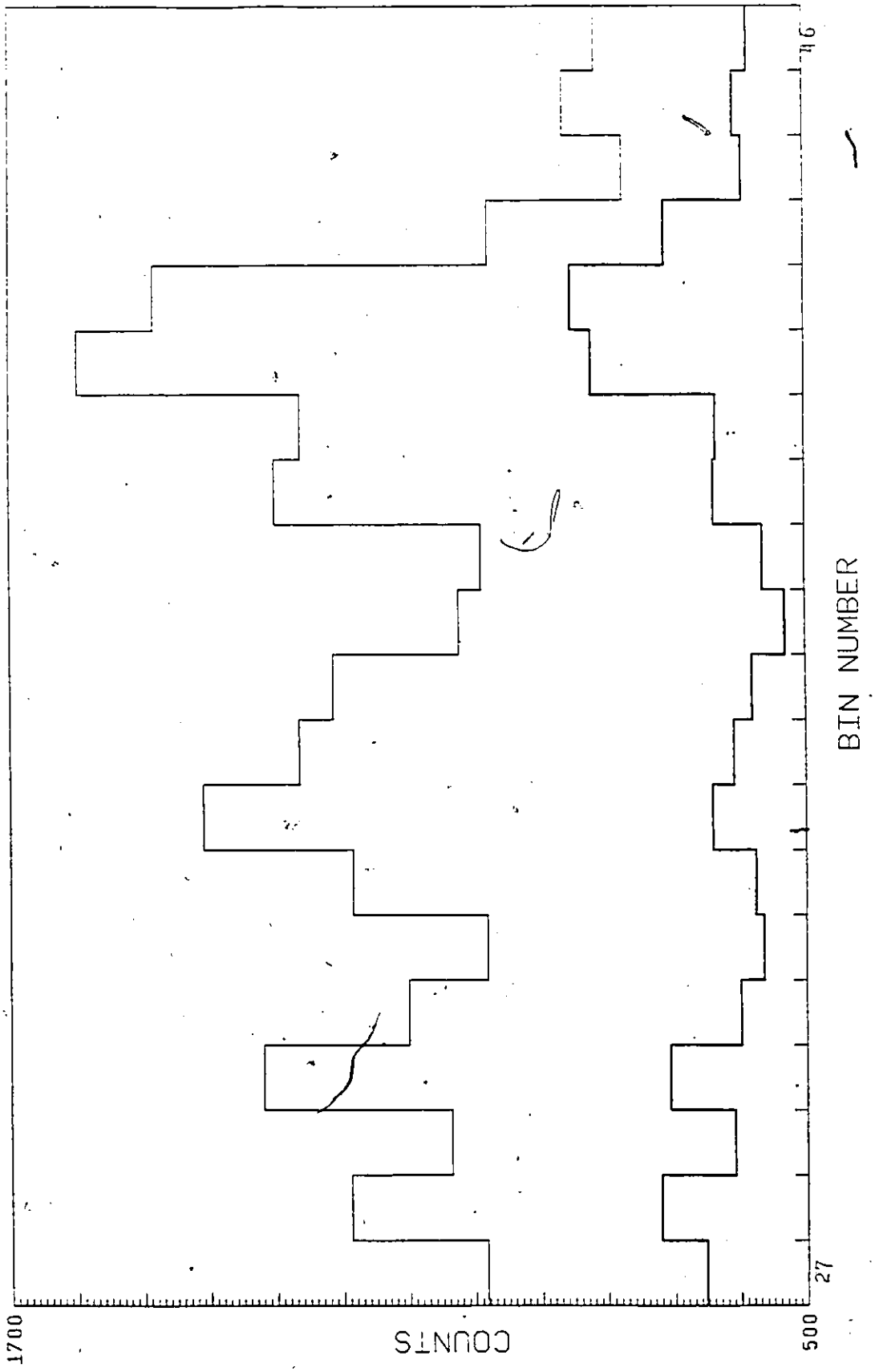
1700
COUNTS
500
27
BIN NUMBER
416

B. Analytical Procedure

The data from any observation of Cir X-1 clearly exhibit fluctuations significantly above those due to photon statistics. Specifically, the variance of the data for an observation normally greatly exceeds that due to photon (Poisson) statistics, namely the mean count rate per bin $\bar{s}$. [For the data in Figure 2, the total variance is $V = 7.3\times10^4$ whereas $\bar{s}$ = 1780 counts/0.320 s.] No previous studies of this source have revealed persistent periodic fluctuations on any time scale. Thus the approach used here to study quantitatively the time variability of aperiodic data is the determination of various statistical moments and correlation functions, as has proved fruitful in the case of Cyg X-1 (Terrell 1972, Sutherland et al. 1978).

The removal of the collimator response and the background from the integer data requires the use of counting statistics corrections. The form of the corrections used parallels the description in Appendix B of Sutherland, Weisskopf, and Kahn (1978) with the necessary modifications due to the data format. The quoted source variances (V), source third moments (M_3), autocorrelation functions (acf), and cross correlation functions (ccf) are with respect to the means ($\bar{s}$).

A slight variation of the standard acf is used in the analysis. If C_i' is the number of CR and background corrected counts in the ith bin, then the acf for the kth lag is

$$\rho_k = \frac{1}{N\langle V\rangle} \sum_{i=1}^{N-k} C_i' C_{i+k}' \qquad (k = 0,1,2,\cdots\cdots,N-1) \qquad (2.1)$$

where N is the total number of bins, and the prime indicates that the mean has been removed. The term <V> refers to the average source variance over many observations. This counting correction alters the standard acf so that the zero lag is not normalized to exactly unity but is approximately so. The averaging factor N, rather than N-k, has been used since it gives a more reasonable acf variance (Jenkins and Watts, 1968).

As previously mentioned, the energy range per channel of the PHA was unclear. However, some spectral information was obtained by defining a hardness ratio (HR) as the ratio of the total counts in the high energy to low energy channels. The arbitrary channel split was chosen such that HR $\sim$ 1. A high-low energy correlation was applied from this.

The cross correlation between the high energy counts (x_i') and the low energy counts (y_i') in the ith bin is given by

$$\rho_{xyk} = \frac{1}{N\sqrt{\langle V_x\rangle\langle V_y\rangle}} \sum_{i=1}^{N+k} x_i' y_{i-k}' \qquad (k = 1-N, 2-N, \cdots, -1, 0) \qquad (2.2)$$

$$\rho_{yxk} = \frac{1}{N\sqrt{\langle V_x\rangle\langle V_y\rangle}} \sum_{i=1}^{N-k} y_i' x_{i+k}' \qquad (k = 1,2,\cdots\cdots,N-1) \qquad (2.3)$$

so that for negative lags the high energy counts precede the low and the reverse is true for positive lags. The prime, as before, indicates that the mean has been removed. Again the average factor N was used and the average variances, $\langle V_x\rangle$

and $\langle V_y \rangle$, were taken over many observations. Similarly, the normalization does not completely restrict values between -1 and +1.

The analysis of the 5 ms data took the following form. For each minor frame the first three moments and a χ^2 value were determined then averaged over the observation. A Poisson distribution based on the mean count per bin was also calculated for each minor frame then averaged over the entire observation. The resultant distribution could then be compared to the histogrammed count rates. As in the scan mode data, an acf per observation was produced and all observations with CR < 10% omitted.

C. Observations

Cir X-1 was observed between Aug. 22 and Sept. 1, 1977 by HEAO-1. Approximately 300 observations of length $\sim$ 12 s each and time resolution 0.320 s were collected of which $\sim$ 170 observations were used in the analysis. An additional 20 observations in the 5 ms point-scan mode have been retained for analysis.

Scan Mode (0.320 s)

The average number of counts per observation per 0.320 s is plotted against time in Figure 3. It is evident that there are several distinct activity levels over the $\sim$ 8 days of data. The average moments per 0.320 s bin for each section

Figure 3. Average Count Rate Per Observation Per 0.320 s for All Observations

The plotted count rates in the high and low energy channels (background and collimator response removed) extend over ∿ 8 days from August 22.65 to August 30.98, 1977. Four sections in time, based on count rates and hardness ratios, were selected for individual analysis. These sections are approximately defined as i) 0-25 hours, ii) 25-130 hours, iii) 130-160 hours, and iv) 160-200 hours. The time axis zero is identically equal to August 22.65, 1977.

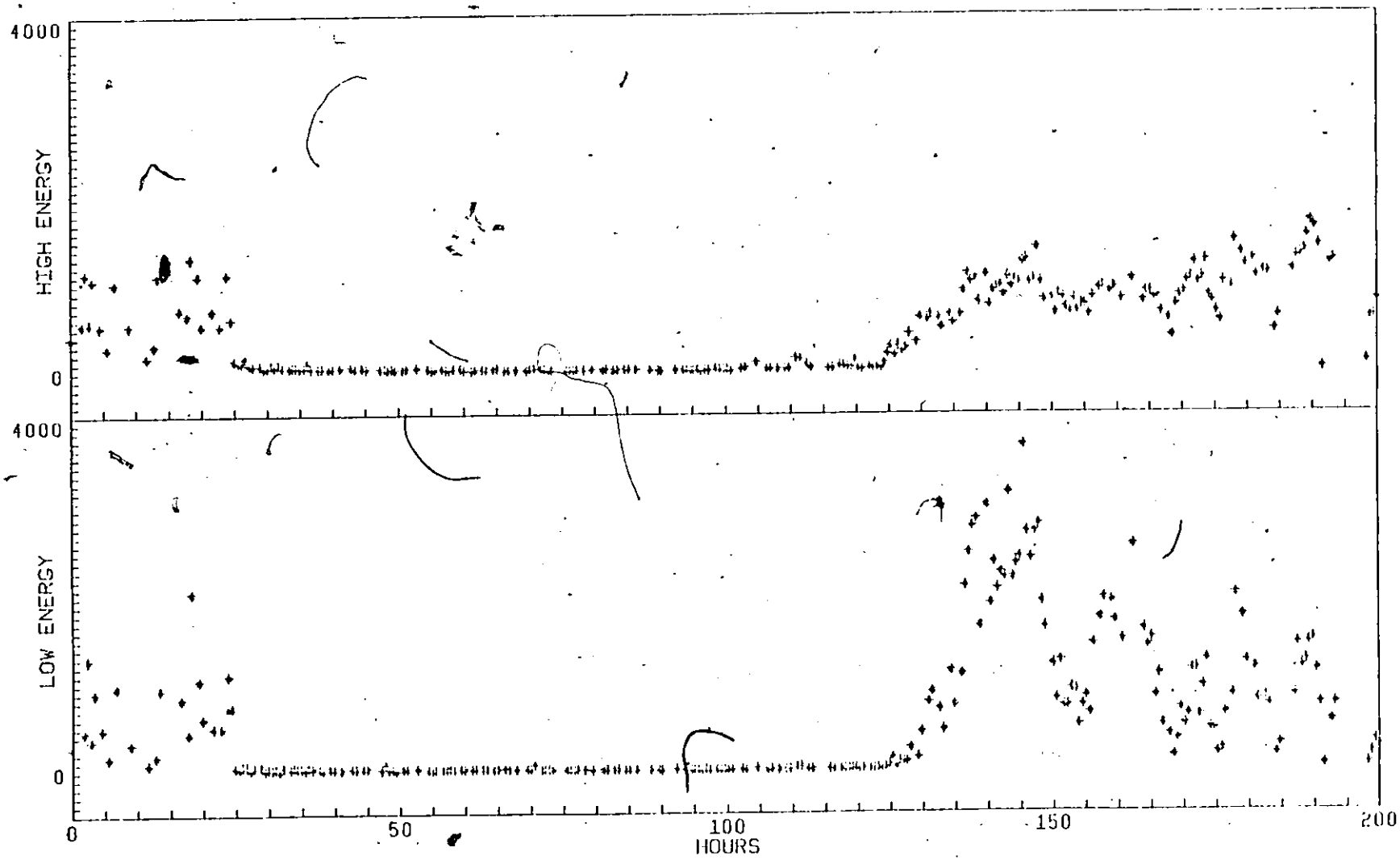
4000
HIGH ENERGY
0
4000
LOW ENERGY
0
0
50
100
150
200
HOURS

of the data chosen are listed in Table 1 along with a distance independent "noise" parameter R, defined as the ratio of the source variance to the square of the mean count rate. It is quite large for the first two sections but drops an order of magnitude for the last two. The latter are still > 10 times higher than those reported by Weisskopf and Sutherland (1980).

Since the "off" or low activity state seen in Figure 3 precludes a meaningful grand averaging, each section, with its own characteristics, will be dealt with in turn.

(i) August 22.65 - August 23.67, 1977. The first section (Figure 4) exhibits rapid fluctuations in the total count rate (factors of 2 in $\leq$ 0.5 h), for the $\sim$ 24 h period that precedes the "off" state. The average total count rate, however, is somewhat low in comparison to those observations beyond the off state (Table 1). One observation is particularly interesting in that the low energy count rate increases to 5 times the value of the previous one. The corresponding high energy band rises by only a factor of $\sim$ 2 giving an overall drop in the HR.

The HR undergoes up to factors of 3 changes in this section averaging to a value greater than unity. The general trend is towards a reduced HR as the total count rate increases.

The autocorrelation function (acf) for this section (Figure 8) illustrates a relatively strong positive value out to lag 3 dropping to negative values at later lags. The cross correlation analysis between the high and the low energy

Section	Day Range*	No. OBs.	Band	$\bar{s}$	V ($\times 10^4$)	M_3 ($\times 10^6$)	R	τ
(i)	22.65-23.67	20	Low	697±102	12.1±1.9	15±11	0.25±.05	
			High	725±72	8.9±1.8	4±6	0.17±.04	
			Total	1423±170	39.6±6.9	54±63	0.20±.04	0.94
(ii)	23.69-27.80	42	Low	13.4±1.9	0.021±.010	0.02±.02	1.2 ±.6	
			High	38.4±6.4	0.046±.098	0.01±.02	0.3 ±.7	
			Total	51.9±8.0	0.121±.023	0.05±.05	0.5 ±.1	0.28
(iii)	27.83-28.99	43	Low	1533±160	21.5±3.7	-1±19	0.09±.02	
			High	772±48	3.0±0.4	2.0±0.8	0.050±.007	
			Total	2306±206	36.7±0.6	23±39	0.069±.006	0.82
(iv)	29.02-30.98	58	Low	962±72	7.9±1.1	2±3	0.085±.012	
			High	973±38	4.2±0.3	3±1	0.044±0.004	
			Total	1935±98	21.2±0.2	2±1	0.057±0.003	0.56

TABLE 1 Time Variability Statistics for All Observations

*Dates are for August 1977

For any statistic, $\bar{s}$, V, or M_3, the error listed is the error in the mean, for the number of observations (column 3), used to determine the statistic.

The last column lists the time constant, τ, determined from shot noise analysis, where the 2σ upper limit to M_3 was included.

bands shows an asymmetry about zero lag. The stronger negative lag indicates a tendency for a high energy count to be followed by a low energy count.

The background is steady at ∿ 20 and ∿ 104 counts per observation per 0.320 s in the low and high energy bands respectively. This background rate remains constant throughout the ∿ 8 days and is within statistical fluctuations expected for a steady background.

(ii) August 23.69-August 27.80, 1977. The onset of the off state occurred on August 23.67 (Figure 5), the count rate dropping by a factor of ∿ 8 in less than 33 m. The low average count rate of 0.025 photons cm^{-2} s^{-1} over both energy bands lasts for ∿ 4.1 d contributing to occasional peaks in the HR. During this period the source went below detection level about 60% of the time mostly within ∿ 32 h from the transition.

Although the low energy band remains relatively constant, the high energy band shows a minimum at the center of the off state, rising towards the beginning and end of the section. The total of the two bands also shows this trend and is consistent with the large but constant HR indicating a high energy dominance in this state.

The off state is reminiscent of the 16.6 d period intensity drops seen in previous work. A least squares fit to first order of 16 transition dates by Dower (1978) gave the result

$$T = 1977 \text{ May } 28.42 \text{ d} \pm n(16.62 \text{ d}) \qquad (2.4)$$

where 1977 May 28.42 = JD 2,443,291.920 with an rms deviation of 0.65 d.

Taking the transition time as the last "on" observation, as defined previously (Kaluzienski et al. 1976, Dower 1978), then this corresponds to the last observation of the preceding section, Aug. 23.67 or JD 2,443,379.17 with an error of ± 0.02 d. This date is ∿ 4 d after the transition predicted from a 16.62 d period with n = 5 and, therefore, cannot be uniquely identified as a periodic transition.

The acf is much weaker than in section (i) but the general shape remains (Figure 9). The ccf continues to be strong about zero lag but drops considerably at early and late lags (Figure 9). The average form of the ccf still displays asymmetry with higher correlation at negative lags.

The separation of sections (iii) and (iv) (Figures 6 and 7) is based on both counting rates and HR. The emergence from the off state gives a gradual rise in the count rate producing a large wide peak. The count rate then decreases followed by more erratic behaviour. The HR, on the other hand, is low and constant over the first peak and then fluctuates afterward. The split is defined as the end of the first peak.

(iii) August 27.83 - August 28.99, 1977. This section lasts for ∿ 28 h with an average flux of 1.07 photons cm^{-2} s^{-1}. It rises from the off state in ∿ 16 h by a factor ≥ 20, then drops

by a factor $\sim$ 3 in < 11 h (see Figure 6).

The HR is initially high ($\sim$ 2.7) then drops by a factor of $\sim$ 4 within 6 h, remaining relatively constant to the end of the section. The contrasting behaviour between the count rate and the HR suggests that this section is strongly dominated by the low energy band. The trailing end of the section, while having a decreasing flux, displays a small but noticeable rise in the HR just before entering section (iv).

The acf and ccf show strong correlations although the former drops quickly as shown in Figure 10. The ccf asymmetry mentioned in section (i) is more pronounced here with negative lag values remaining above zero throughout and with the positive lags dropping rapidly. The acf's and the ccf's for individual observations exhibit stronger correlations when the mean count rate is high in this section. The correlations seem to be related to the total count rate although the last two observations in particular have strong acf's and ccf's but a low flux and a HR close to unity.

(iv) <u>August 29.02 - August 30.98, 1977</u>. The rather smooth shape of the count rate in (iii) leads into a more varying area containing several peaks (Figure 7). The section has an average count rate over the $\sim$ 2d period of 0.916 photons cm^{-2} s^{-1} which is slightly lower than section (iii). Note that the first peak in the low energy band has only a small complement in the high energy band. The variability of the total flux is

seen in the HR over the section.

The opposing trends between the count rate and the HR continues here in a more obvious manner. The HR gradually rises with both bands contributing but with the high band leading in time by ∿ 30 m.

The acf again drops to negative values at later lags (Figure 11) but far less steeply than in (iii). The overall ccf is high at zero lag with strong asymmetric values about zero lag (Figure 11). Late positive lags become slightly negative whereas the late negative lags remain above zero. Several sharp peaks in the total count rate, that tend to correspond to low HR values, are also evident in the individual acf's and ccf's. The peaks often give strong acf's out to about lag 4 and asymmetric ccf's with large positive values out to lag 5 and negative values past lag 2. This trend is contradicted by an increase in the low band by a factor of ∿ 2 about 9.5 h into this section. The acf for this observation is very strong at lag 1, almost zero at lag 2, then drops below zero until reaching another peak positive value at lag 8. The corresponding ccf is large and positive only for lags $-2 \leq k \leq 1$. The burst appears to be restricted in time with delayed after effects.

Figure 4. Average Count Rates for August 22.65-August 23.67, 1977.

The count rates for both the low and high energy bands and the corresponding hardness ratios are averages taken per observation per 0.320 s. The time axis zero is identically equal to August 22.65, 1977. For subsequent sections, the time axis zero is equal to the first date of the given calendar range.

SECTION ONE

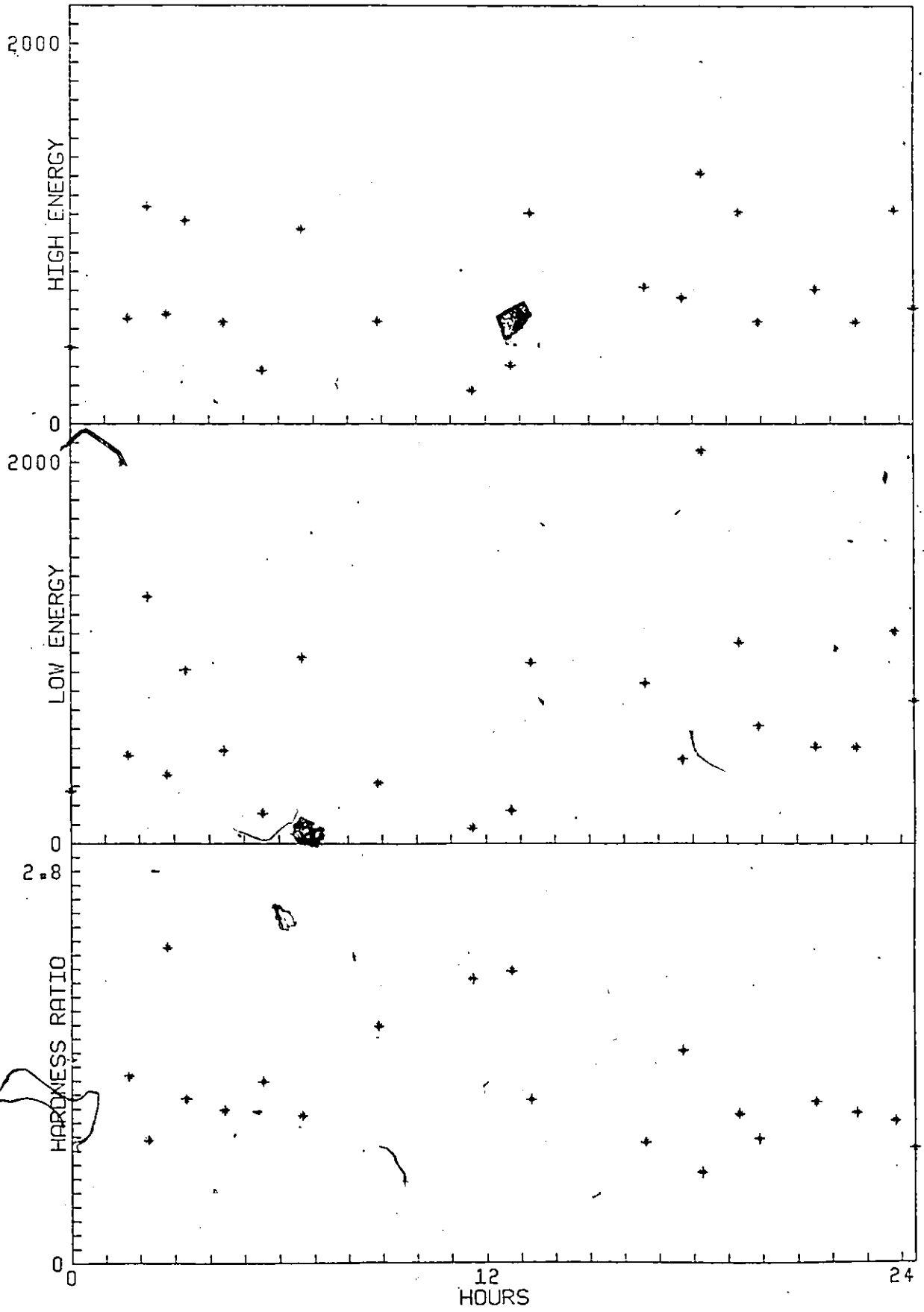
2000
HIGH ENERGY
0
2000
LOW ENERGY
0
2.8
HARDNESS RATIO
0
0
12
24
HOURS

Figure 5. Average Count Rates for August 23.69-August 27.80, 1977.

SECTION TWO

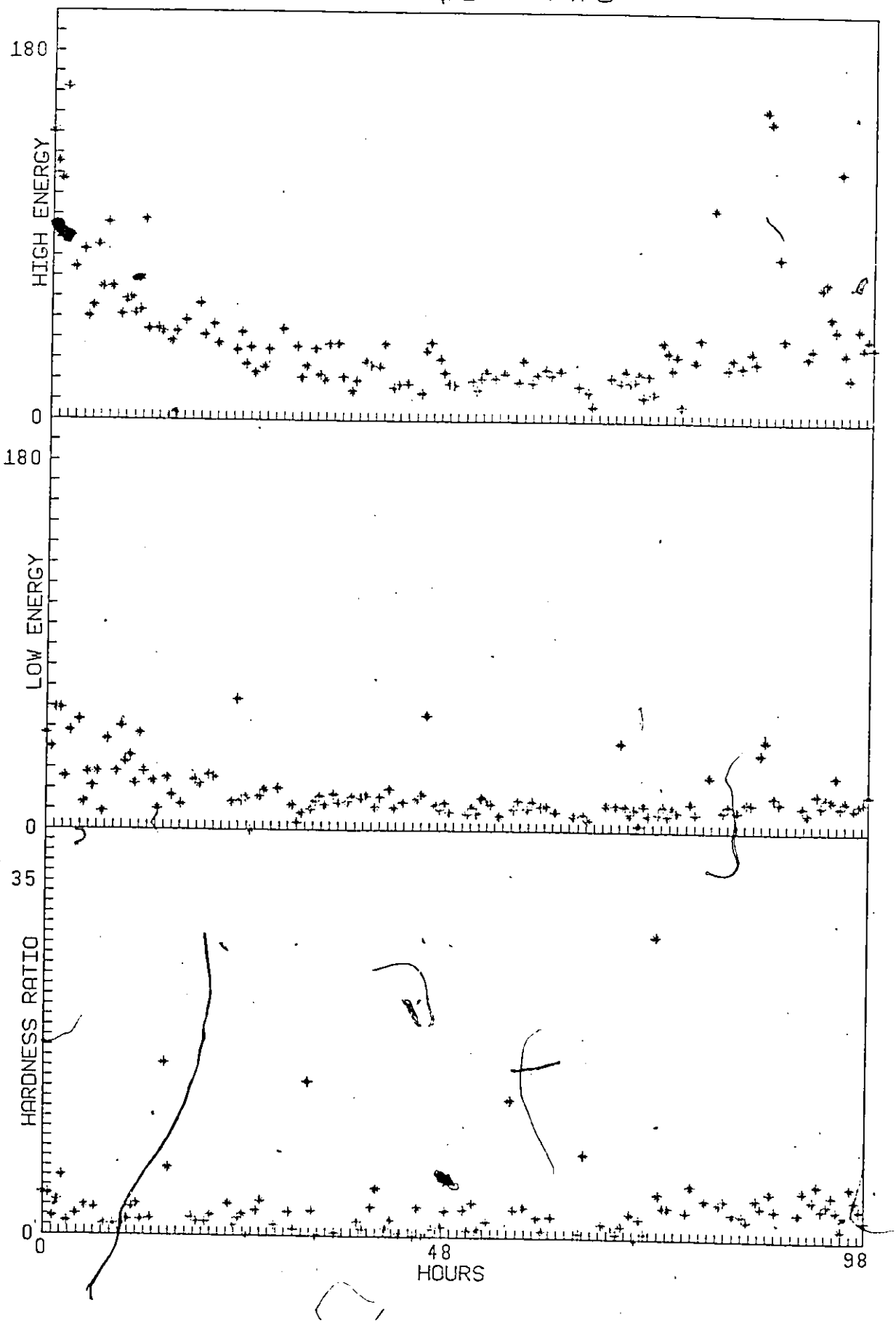
180
HIGH ENERGY
0
180
LOW ENERGY
0
35
HARDNESS RATIO
0
0
48
HOURS
98

Figure 6. Average Count Rates for August 27.83-August 28.99, 1977.

SECTION THREE

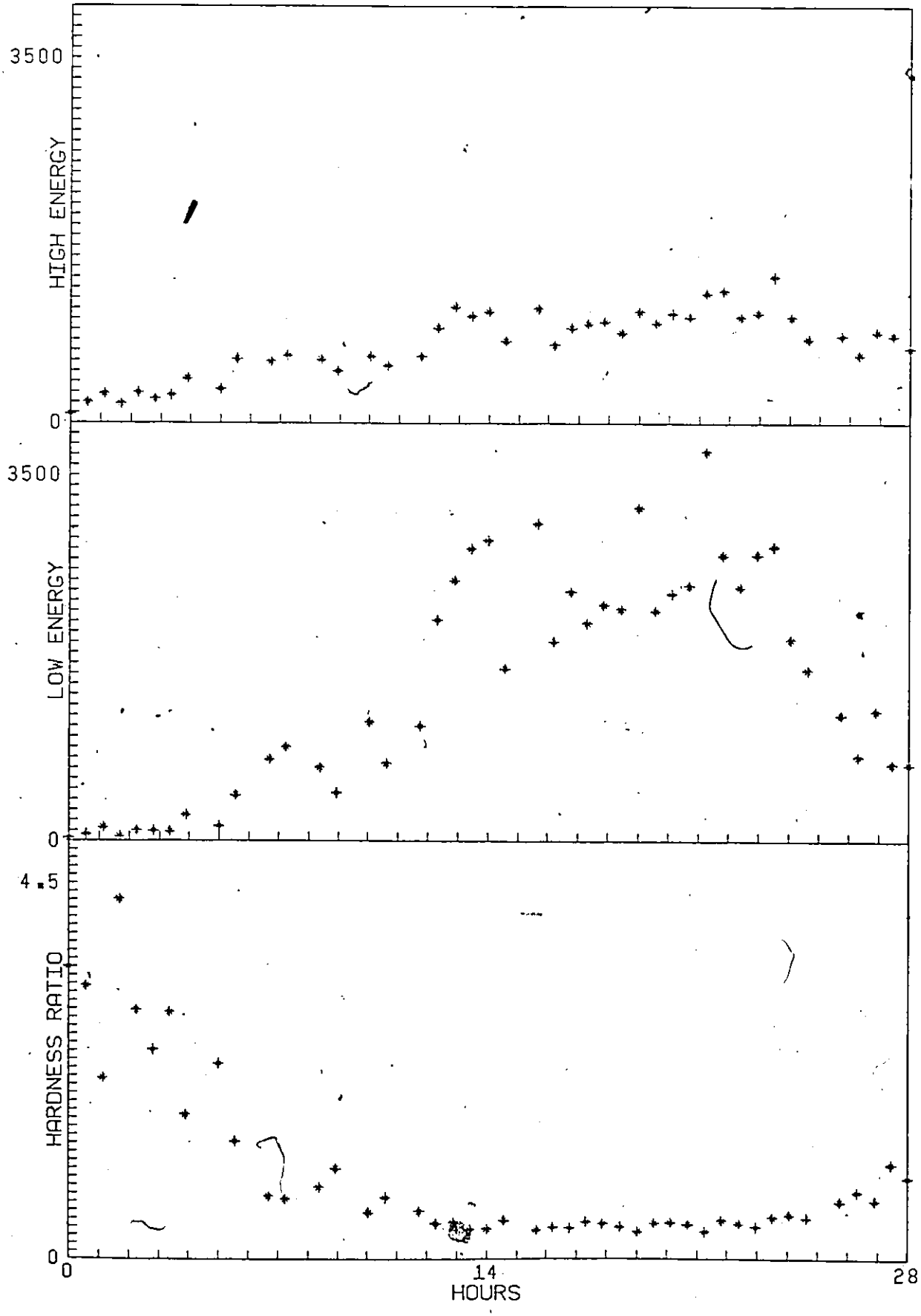

Figure 7. Average Count Rates for August 29.02-August 30.98, 1977.

SECTION FOUR

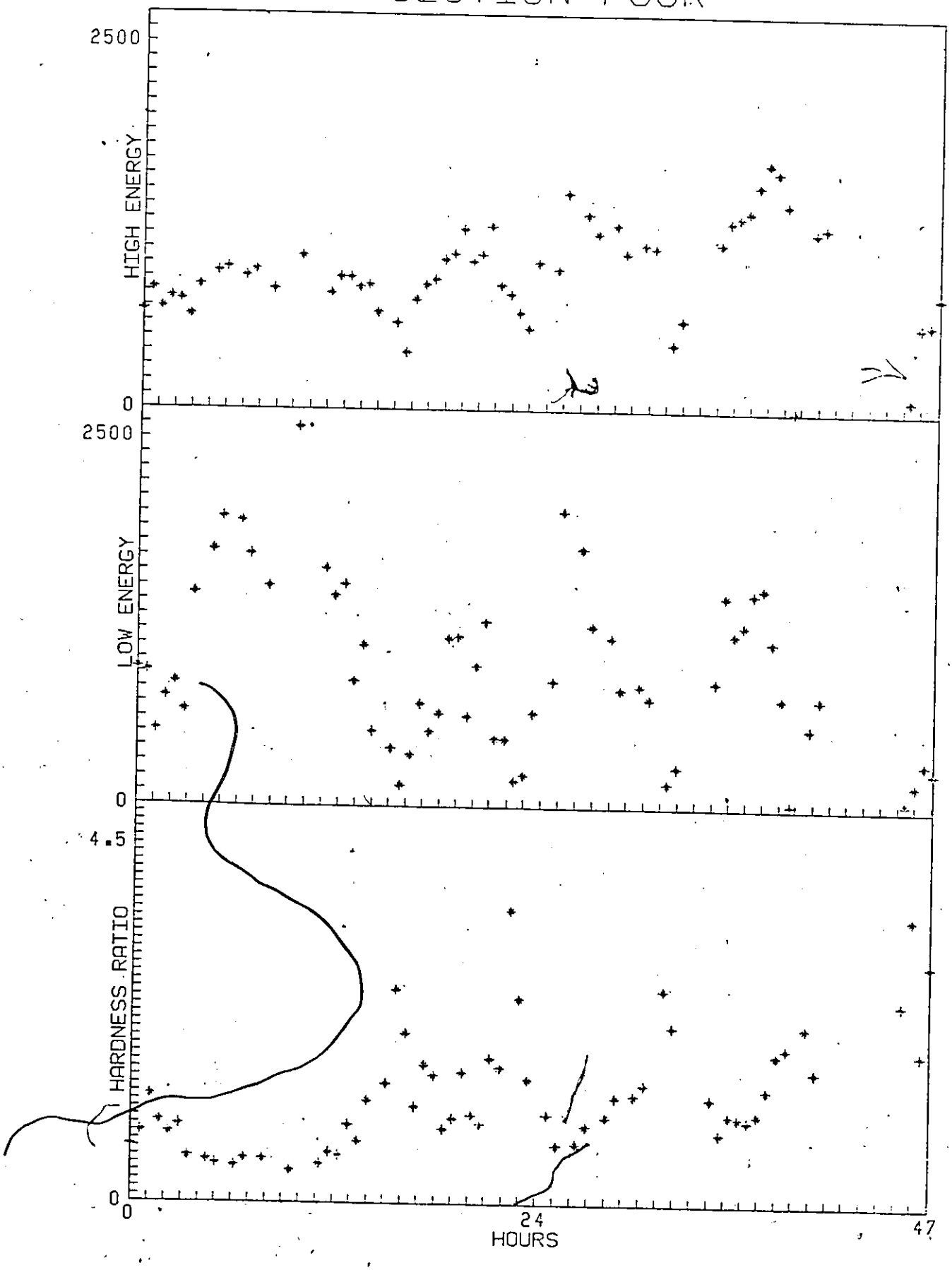

Figure 8. Average Autocorrelation and Cross Correlation Functions for August 22.65-August 23.67, 1977. The lag number is the time delay in units of 0.320 s. As mentioned in the text, the determined zero lag value for the autocorrelation function is not exactly unity. It is set to 1, here, for convenience. The error quoted is the typical 2σ error.

SECTION ONE

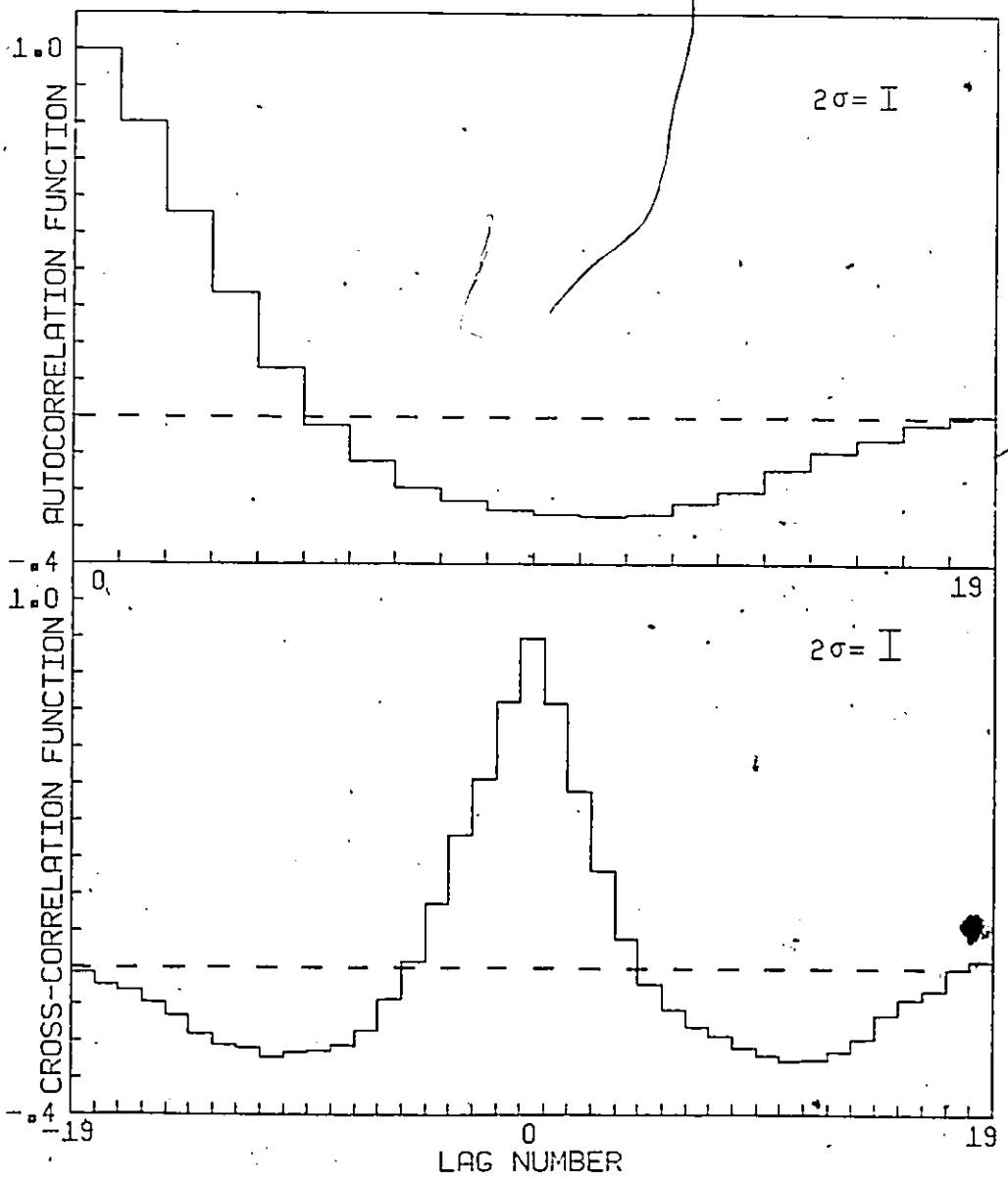
1.0
AUTOCORRELATION FUNCTION
2σ= I
-.4
0
19
1.0
CROSS-CORRELATION FUNCTION
2σ= I
-.4
-19
0
19
LAG NUMBER

Figure 9. Average Autocorrelation and Cross Correlation Functions for August 23.69-August 27.80, 1977.

SECTION TWO

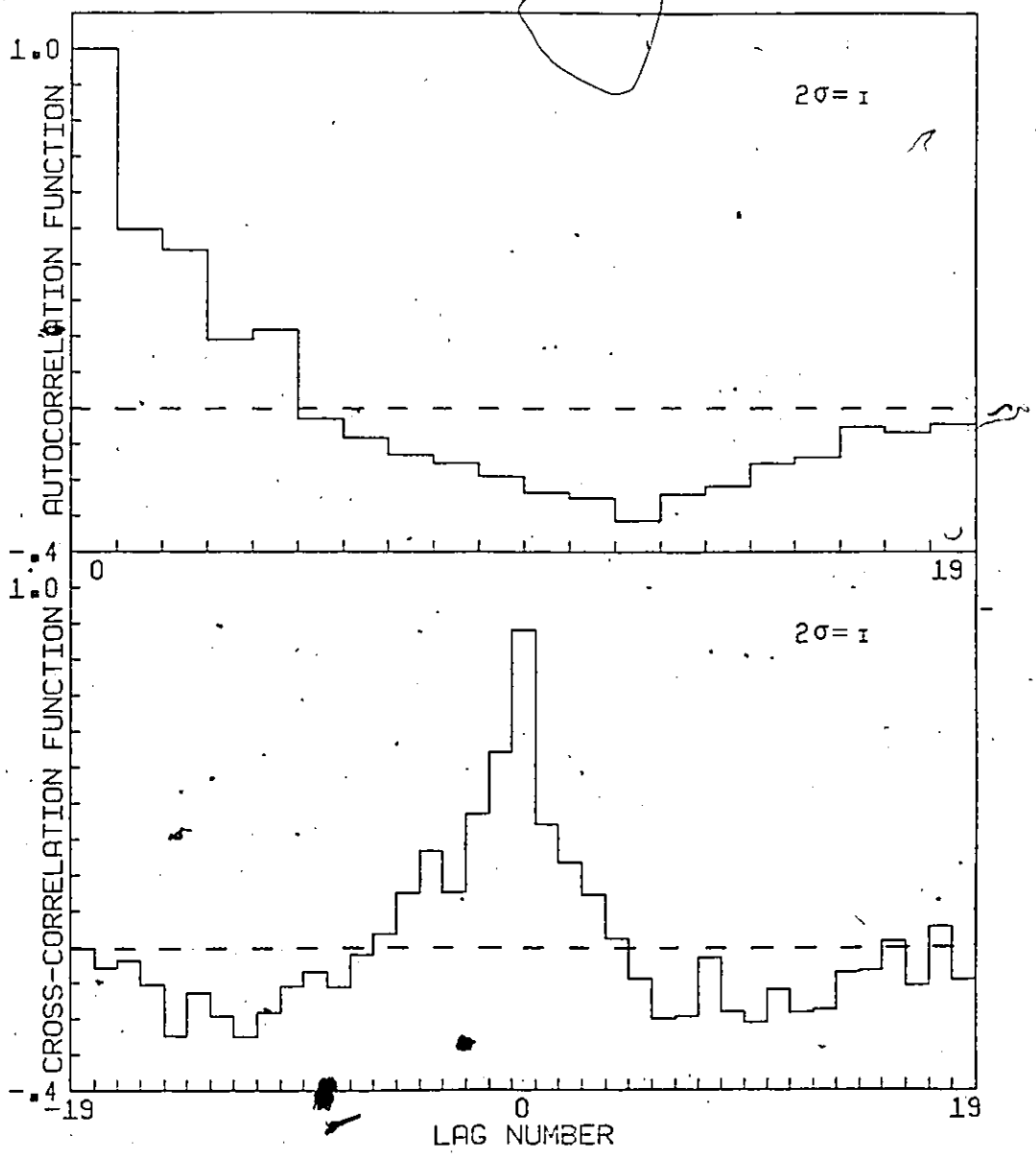
1.0
AUTOCORRELATION FUNCTION
2σ= 1
-.4
0
19
1.0
CROSS-CORRELATION FUNCTION
2σ= 1
-.4
-19
0
19
LAG NUMBER

Figure 10. Average Autocorrelation and Cross Correlation Functions for August 27.83-August 28.99, 1977.

SECTION THREE

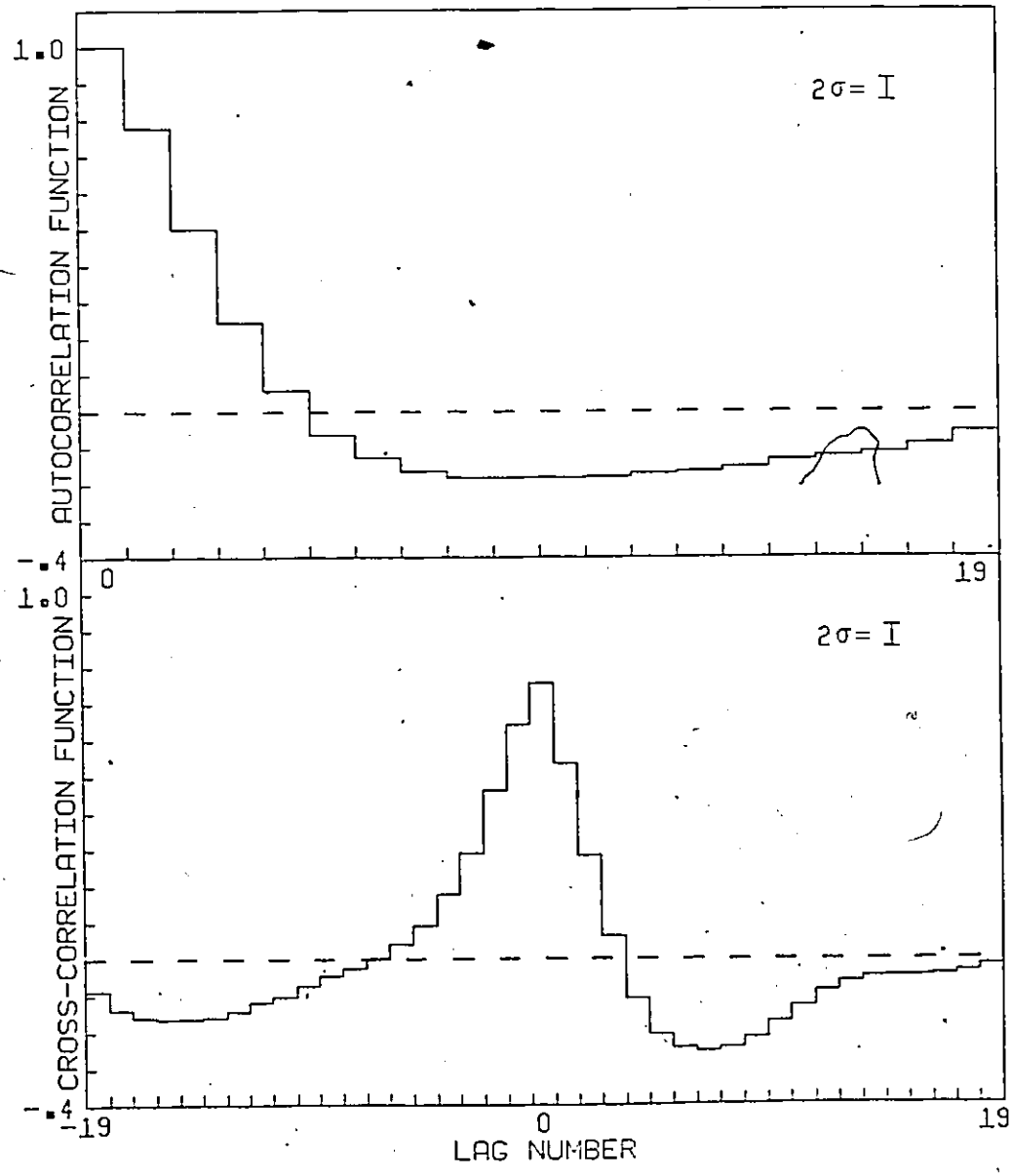

Figure 11. Average Autocorrelation and Cross Correlation Functions for August 29.02-August 30.98, 1977.

SECTION FOUR

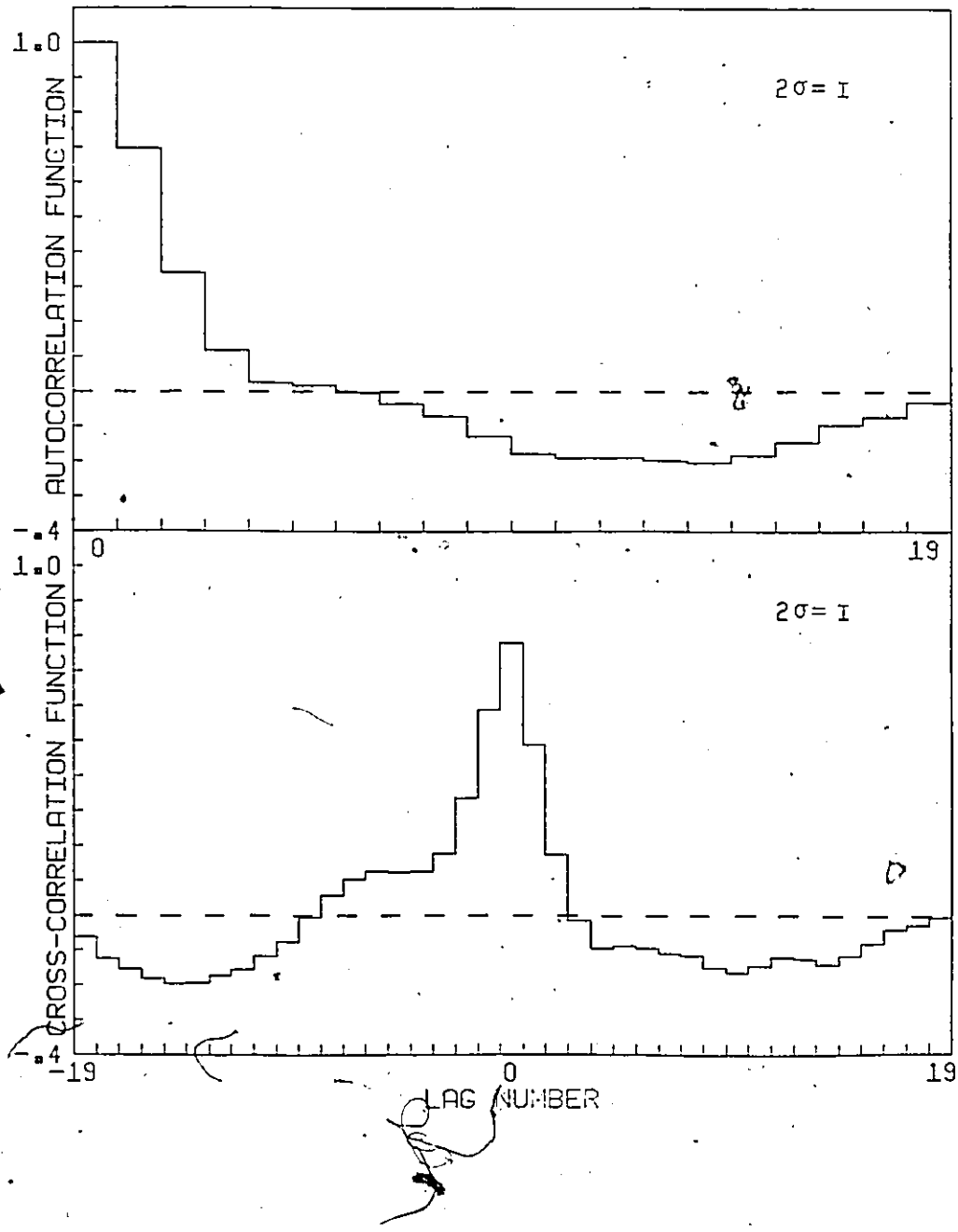

Shot Noise Analysis

In a shot noise model for the time variability of an aperiodic X-ray source, the variability is attributed to shots or flares that occur randomly in time at a rate λ. The individual shots have a characteristic correlation time τ and a strength or integrated flux Q ($Q \sim h\tau$ where h is the maximum instantaneous intensity). It is presumed that the average flux of the shots is some fraction $\alpha \leq 1$ of the total average flux, the remaining fraction $(1-\alpha)$ of the flux is due to a steady component. Thus these four parameters completely characterize a model of the data. They may be determined from the data if a specific shape is assumed for the shot, although the parameters are not strongly shape dependent. Sutherland, Weisskopf, and Kahn (1978) give formulae for the case of exponential shots which we repeat below.

$$\begin{aligned} \bar{s} &= (\lambda h\tau + c)T \\ V &= \lambda h^2\tau^3(x - 1 + e^{-x}) \\ M_3 &= \lambda h^3\tau^4(x - \tfrac{3}{2} + 2e^{-x} - \frac{e^{-2x}}{2}) \\ \rho_k' &= (\frac{2\sinh^2(x/2)}{x-1+e^{-x}})e^{-kx} \end{aligned} \qquad (2.5)$$

where c is the steady component, ρ_k is the acf for the kth lag, T is the time width of the binning, and $x = T/\tau$. In principle, the statistics on the left hand side are obtained from the data, with due account taken of the contribution due to photon counting statistics. The four parameters of Eqns. 2.5 (λ,h,τ,c)

cannot be solved for analytically but a self-consistent approach to the equation in ρ_k yields x_0 (or equivalently τ) from which the others readily follow.

The exponential shot model failed to characterize the source by giving a shot fraction greater than unity when the total energy band moments (Table 1) were used. Reasonable parameters were obtained however by utilizing the 2σ upper limit to M_3 as tabulated in Table 2. Except for the off state value, Table 2 shows a high uniform shot fraction. Again, these values are derived from reasonable upper limits on M_3 and are lower limits for the shot fraction and λ, and upper limits for the shot strength.

Point-scan Mode (5 ms)

The 5 ms data contained 34 observations that were obtained between August 30.72 and August 31.66, 1977. Based on the CR criteria, (peak collimator response > 0.1) only 20 observations were used in the analysis.

To test for time variability on time scales shorter than 0.320 s (one minor frame) a χ^2 variable was calculated for each observation (20 minor frames). This was taken to be

$$\chi^2 \equiv \sum_{i=1}^{64} \frac{(n_i - \bar{n})^2}{\bar{n}} \qquad (2.6)$$

where $\bar{n}$ is the average count rate per 5 ms bin for a given minor frame. The effective number of degrees of freedom is $\nu = 63$, and so the average value of χ^2 over the 20 minor frames

Section	λ (shots s^{-1})	$h\tau$ (counts)	Shot Fraction (%)
(i)	1.5	2300	80
(ii)	0.2	240	25
(iii)	4.5	1200	75
(iv)	8.0	600	80

TABLE 2 Shot Noise Parameters

Because the shot noise parameters are in part determined by M_3, which is poorly known in this table, parameters are calculated by using the 2σ upper limit to M_3 (for the total energy band). If a smaller value is used for M_3, then λ increases, $h\tau$ decreases, and the shot fraction increases.

should be 63 with an error in the mean $\sqrt{2\sigma/20} \approx 2.5$, if the only variability in the counts was that due to photon statistics. Significantly larger values of χ^2 would suggest time variability intrinsic to the source on short time scales. An expected average χ^2 value per observation of 63 was exceeded by greater than 3σ ($\sigma \sim 2.5$) in 10 of the 20 observations. Several of these observations (5) reached average deviations beyond 6σ.

Most of the statistically significant deviations in χ^2 were reflected in data histograms. High χ^2 values corresponded to histogram counts in the tail > 20 times that expected from Poisson statistics. In contrast, the averaged acf per observation showed no obvious trends or consistent correlations at any lag. Histogrammed 5 ms counts from a sample high $\langle\chi^2\rangle$ observation are tabulated against the expected Poisson counts with the same mean (Table 3). The data show little difference at low count rates but there are instances of high rates above those predicted by a Poisson distribution.

The conclusions that can be drawn from an examination of the χ^2 values and significant departures (when present) from the expected Poisson counts are: (i) occasional very large flares or spikes, unresolved at the 5 ms level, occur, and (ii) in many observations (or large fractions thereof) the 5 ms data are significantly noisier than photon statistics, but show no clear correlations on short time scales and have no especially large flares or spikes.

Data		Poisson
Counts	Frequency	Expected Frequency
0	41	33
1	116	94
2	154	151
3	185	181
4	154	184
5	164	166
6	127	138
7	103	108
8	82	80
9	48	56
10	36	37
11	23	23
12	18	13
13	13	7.4
14	9	4.0
15	4	2.0
16	1	0.9
17	0	0.4
18	1	0.2
19	0	0.07
20	0	0.03
21	0	0.01
22	1	0.003
23	0	0.001
24	0	0.0003
25	0	0.0001

TABLE 3. Histogrammed 5 ms Data and Poisson Expected Counts for 1 Observation

The above data have an $\langle \chi^2 \rangle = 82 \pm 13$ and a mean = 4.86. This mean determined the Poisson counts.

III. DISCUSSION

The results of the data analysis show that Cir X-1 exhibits time variability from the millisecond level to days. Several features are similar to those found for Cyg X-1 while others seem unique to Cir X-1.

The quick intensity dip ($\lesssim$ .33 m) and slow rise ($\sim$ 3 d) of the "off" state are reflected in both the high energy and low energy bands and do not strongly affect the previously high cross correlation between the bands. The reduction of the autocorrelation function at all lags may indicate an energy degradation of emitted photons by absorbing material about the source.

The change in the hardness ratio from before the dip to about mid-point in the off state is uncertain enough that a constant spectrum is consistent with the data.

The predicted transition data, based on a 16.62 d period (Dower 1978), however is $\sim$ 4 d before the onset of the off state seen here. The $\sim$ 4% deviation of prior transitions about the predicted transitions cannot easily account for the time delay, even though the evidence argues against a simple eclipse phenomenon. On the assumption that the intensity dip is not a 16.6 d transition, there exists a similarity to a post-transition feature evident in earlier work. Intensity dips of an $\sim$ 1 d duration after an identified 16.6 d transition can be seen in two observations in November 1975 and February

1976 given by Kaluzienski et al. (1976) plus one in late February 1976 presented by Wilson and Carpenter (1976). A dip $\sim$ 3 d after transition was reported by Kaluzienski and Holt (1977).

A recent model (Murdin et al. 1979) suggests an explanation for the transition and the post-transition dip. If the compact object is in an eccentric orbit ($e \gtrsim 0.6$) and periastron occurs in front of the primary (with respect to the line of sight), then on approaching periastron the X-ray emission by the compact object increases due to the increased capture of the primary's stellar wind. Near closest approach, X-ray absorption by the stellar wind (now enveloping the source) becomes significant and emission drops rapidly. The binary system is tight enough during periastron passage (of duration $\sim 10^5$ s) that mass transfer from the primary to the compact object occurs. This is a possible mechanism for replenishing the expected accretion disk around the secondary. X-ray emission then gradually increases past periastron as the stellar wind density drops. Emission at this phase is attributed to infalling matter from the accretion disk and/or a stellar wind contribution. As the compact object moves behind the primary, the line of sight includes the dense stellar wind and an intensity drop results. Precession of the orbit has been proposed to explain the increase in lag time between the transition and the post-transition dip.

Fluctuations at the 5 ms level may indicate an X-ray emission region of size $\sim 10^8$ cm which is smaller than a white dwarf size ($\sim 10^9$ cm). However, small, local disruptions in the accretion disk can also give rise to millisecond bursts. Previously determined Cir X-1 luminosities ($\sim 10^{38}$ erg s^{-1}) argue against a white dwarf (Fabian et al. 1976) as the X-ray source. This leaves a neutron star or a black hole as the possible compact object. In addition, the absence of a stable pulse period on short time scales rules against a rotating neutron star with a strong magnetic field.

The lack of a stable pulse period and variability on all time scales are also common to Cyg X-1 (Weisskopf and Sutherland 1980). Both sources also display transitions to low flux followed by radio flares (Whelan et al. 1977), and similar time constants ($0.5 \text{ s} \lesssim \tau \lesssim 1.0 \text{ s}$). Spectral states are also comparable although data beyond 20 keV is lacking for Cir X-1.

In contrast to Cir X-1, Cyg X-1 exhibits infrequent and irregular transitions seemingly unrelated to the 5.6 d orbital period of the primary. The transition characteristics are also different. Cyg X-1 rises rapidly ($\lesssim 1$ d) to the high state and falls slowly (~ 10 d) to the low states. These transitions are possibly due to instabilities in the accretion disk.

Correlations around the 0.320 s level are stronger here than those reported earlier for Cir X-1 (bin size 0.384 s) (Weisskopf and Sutherland 1980). Acknowledging the difference in bin size, the acf's for Cyg X-1 and Cir X-1 are much more similar in shape showing strong correlation at low lags. Furthermore, both sources exhibit asymmetric ccf's with negative lags remaining prominent as compared to positive lags.

Shot model parameters for Cir X-1 remain uninformative. The poor third moments allow only the derivation of 2σ upper limits in M_3 giving shot fractions at the 80% level, far higher that those determined before (Weisskopf and Sutherland 1980). Only the shot strength results are somewhat comparable, discounting those values pertaining to the "off" state.

Certainly more work is necessary to characterize Cir X-1 as a neutron star or black hole, particularly more refined observations of the primary, a more detailed analysis of the X-ray light curve over several 16.6 d periods, and extended short time scale data about the transitions.

At this point Cir X-1 is compared to Cyg X-1 because of their short term emission similarities. The evidence for Cyg X-1 being a black hole is reasonably good. The power of the argument, however, is based solely on one number, the estimated mass of the compact object. For Circinus X-1, the estimated mass used in a recent model (Murdin et al. 1979) of 1 $M_\odot$ is little more than a guess. The mass determination

awaits optical observations of the primary. The reddening of the star's emission and therefore its faintness poses a significant obstacle to this number. Further data from HEAO-2 and a proposed optical satellite will aid the verification and extension of the parameters characterizing Cir X-1.

REFERENCES

Bachall, J.N. 1978, in Annual Review of Astronomy and Astrophysics, ed. G. Burbidge (Palo Alto: Annual Reviews), 16, pp. 241-264.

Bignami, G.F., Della Ventura, A., Maccagni, D., and Stiglitz, R.A. 1977 Astr. and Ap., 57, 309.

Bolton, C.T. 1972, Nature, 235, 271.

Bowyer, C.S., Byram, E.T., Chubb, T.A., and Friedman, H. 1964, Science, 146, 912.

Buff, J., Jernigan, G., Laufer, B., Bradt, H., Clark, G.W., Lewin, W.H.G., Matilsky, T., Mayer, W., and Primini, F. 1977, Ap. J., 212, 768.

Burnight, T.R. 1949, Phys. Rev., 76, 165.

Byram, E.T., Chubb, T.A., and Friedman, H. 1966, Science, 152, 66.

Canizares, C.R., Li, F.K., and Clark, G.W. 1974, Ap. J. (Letters), 191, L75.

Canizares, C.R., McClintock, J.E., and Grindlay, J.E. 1980, Ap. J. (Letters), 236, L55.

Canizares, C.R., and Oda, M. 1977, Ap. J. (Letters), 214, L119.

Clark, D.M., Parkinson, J.M., and Caswell, J.L. 1975, Nature, 254, 674.

Coe, M.J., Engel, A.R., and Quenby, J.J. 1976a, Nature, 259, 544.

Coe, M.J., Engel, A.R., and Quenby, J.J. 1976b, Nature, 262, 563.

Dolan, J.F., Crannell, C.J., Dennis, B.R., Frost, K.J., and Orwig, L.E. 1977, Nature, 267, 813.

Dower, R.G. 1978, MIT Ph.D. Thesis.

Eyles, C.J., Skinner, G.K., and Willmore, A.P. 1975, M.N.R.A.S. 173, 63P.

Fabian, A.C., Pringle, J.E., and Rees, M.J., 1976, M.N.R.A.S. 175, 43.

Giacconi, R., Gursky, H., Paolini, F.R., and Rossi, B.B., 1962, Phys. Rev. Letters, 9, 439.

Giacconi, R., Kellogg, E., Gorenstein, P., Gursky, H., and Tananbaum, H. 1971, Ap. J. (Letters), 165, L27.

Glass, I.S., 1978, M.N.R.A.S., 183, 335.

Goss, W.M. and Mebold, U. 1977, M.N.R.A.S., 181, 255.

Gursky, H., Giacconi, R., Paolini, F.R., and Rossi, B.B. 1963, Phys. Rev. Letters, 11, 530.

Harries, J.R., Tuohy, I.R., Broderick, A.J., Fenton, K.B. and Luyendyk, A.P.J. 1971, Nature Phys. Sci., 234, 149.

Holt, S.S., Boldt, E.A., Serlemitsos, P.J., Kaluzienski, L.J. 1976a, Ap. J. (Letters), 203

Holt, S.S., Kaluzienski, L.J., Boldt, E.A., Serlemitsos, P.J. 1976b, Nature, 261, 213.

Jenkins, G.M. and Watts, D.G. 1968, Spectral Analysis and its Applications, (San Francisco: Holden-Day), pp. 140-208.

Jones, C., Giacconi, R., Forman, W., and Tananbaum, H. 1974, Ap. J. (Letters), 191, L71.

Kaluzienski, L.J. and Holt, S.S. 1977, IAU Circ. No. 3106.

Kaluzienski, L.J., Holt, S.S., Boldt, E.A., and Serlemitsos, P.J. 1976, Ap. J. (Letters), 208, L71.

Kellogg, E.M. 1973 in Proc. I.A.U. Symposium No. 55, X- and Gamma-ray Astronomy, ed. H. Bradt and R. Giacconi (Dordrecht:Reidel), p. 171.

Lewin, W.H.G., Doty, J., Clark, G.W., Rappaport, S.A., Bradt, H.V.D., Doxsey, R., Hearn, D., Hoffman, J., Jernigan, J., Li, F., Mayer, W., McClintock, J., Primini, F., and Richardson, J. 1976, Ap. J. (Letters), 207, L95.

Margon, B., Lampton, M., Bowyer, S., and Cruddace, R. 1971, Ap. J. (Letters), 169, L23.

Mayo, S.K., Whelan, J.A.J., and Wickramasinghe, D.T. 1976, IAU Circ. No. 2957.

Murdin, P., Haynes, R.F., Jauncey, D.L., Lerche, I., Nicolson, G.D., Holt, S.S., and Kaluzienski, L.J. 1979, submitted to Astr. and Ap.

Murdin, P. and Webster, B.L. 1971, Nature, 233, 110.

Osmer, P.S., Hiltner, W.A., Whelan, J.A.J. 1975, Ap. J., 195, 705.

Rappaport, S., Doxsey, R., and Zaumen, W. 1971a, Ap. J. (Letters), 168, L43.

Rappaport, S., Zaumen, W., and Doxsey, R. 1971b, Ap. J. (Letters), 168, L17.

Rothschild, R.E., Boldt, E.A., Holt, S.S., and Serlemitsos, P.J. 1974, Ap. J. (Letters), 189, L1.

Sadeh, D., Meidav, M., Wood, K., Yentis, D., Smathers, H., Meekins, J., Evans, W., Byram, E.T., Chubb, T.A., Friedman, H. 1979, Nature, 278, 436.

Sandage, A.R., Osmer, P., Giacconi, R., Gorenstein, P., Gursky, H., Waters, J.R., Bradt, H., Garmire, G., Sreekantan, B.V., Oda, M., Osawa, K., and Jukago, J. 1966, Ap. J., 146, 316.

Sommer, M., Maurus, H., and Urbach, R., 1976, Nature, 263, 752.

Spada, G., Bradt, H., Doxsey, R., Levine, A. and Rappaport, S. 1974, Ap. J. (Letters), 190, L113.

Sutherland, P.G., Weisskopf, M.C., Kahn, S.M. 1978, Ap. J., 219, 1029.

Tananbaum, H., Gursky, H., Kellogg, E., Giacconi, R., and Jones, C. 1972, Ap. J. (Letters), 177, L5.

Terrell, N.J., Jr. 1972, Ap. J. (Letters), 174, L35.

Toor, A. 1977, Ap. J. (Letters), 215, L57.

Tuohy, I.R. and Davison, P.J.N. 1973, Nature Phys. Sci., 244, 121.

Walborn, N.R. 1973, Ap. J. (Letters), 179, L123.

Webster, B.L. and Murdin, P. 1972, Nature, 235, 37.

Weisskopf, M.C., and Sutherland, P.G. 1980, Ap. J., 236, 263.

Weisskopf, M.C., Sutherland, P.G., Katz, J.I., and Canizares, C.R. 1978, Ap. J. (Letters), 223, L17.

Whelan, J.A.J., Mayo, S.K., Wickramasinghe, D.T., Murdin, P.G., Peterson, B.A., Howarden, T.G., Longmore, A.J., Haynes, R.F., Goss, W.M., Simons, L.W., Caswell, J.L., Little, A.G. and McAdam, W.B. 1977, M.N.R.A.S., 181, 259.

Wilson, A.M. and Carpenter, G.F. 1976, Nature, 261, 295.